Competing Ground States of Metal-Halide Ladders

Kei-ichi Funase and Shoji Yamamoto
Division of Physics, Hokkaido University, Sapporo 060-0810, Japan

(Dated: 26 January 2006)

Based on a symmetry argument, we investigate the ground-state properties of newly synthesized metal-halide ladder compounds $(C_8H_6N_4)[Pt(C_2H_8N_2)X]_2(ClO_4)_4{\cdot}2H_2O$ ($X = Cl, Br, I$). Employing a fully dressed two-band Peierls-Hubbard model, we systematically reveal possible charge- or spin-ordered states. Numerical phase diagrams demonstrate a variety of competing Peierls and Mott insulators with particular emphasis on the transition between two types of mixed-valent state of Pt^{II} and Pt^{IV} driven by varying interchain hopping integrals and Coulomb interactions.

PACS numbers: 71.10.Hf, 71.45.Lr, 75.30.Fv

I. INTRODUCTION

The family of quasi-one-dimensional transition-metal (M) complexes with bridging halogens (X) has been attracting much interest for several decades.[1,2] They present an exciting stage performed by electron-electron correlation, electron-lattice interaction, low dimensionality and d-p orbital hybridization, because their electronic state is widely tunable, substituting the metals, halogens, ligand molecules and counterions. The well-known Wolffram red salt $[Pt(ea)_4Cl]Cl_2{\cdot}2H_2O$ (ea = ethylamine = C_2H_7N)[3] possesses a Peierls-distorted mixed-valent ground state. Its emission spectrum is so interesting as to consist of highly resonant Raman lines and a remarkably Stokes-shifted luminescence band.[4,5] A nickel analog $[Ni(chxn)_2Br]Br_2$ (chxn = cyclohexanediamine = $C_6H_{14}N_2$)[6,7] has a Mott-insulating monovalent regular-chain structure, but the bridging bromine ions can be photoexcited into polarons.[8] The competition between Peierls and Mott insulators[9] is more impressively observed in mixed-metal compounds $[Ni_{1-x}Pd_x(chxn)_2Br]Br_2$ ($0 \le x \le 1$).[10,11] Metal binucleation stimulates further interest in the MX family. Two types of diplatinum-halide chain compounds, $A_4[Pt_2(pop)_4X]{\cdot}nH_2O$ ($X = Cl, Br, I$; $A = Li, Cs, \cdots$; pop = diphosphonate = $P_2O_5H_2$)[12,13] and $Pt_2(RCS_2)_4I$ (R = alkyl chain = C_nH_{2n+1})[14,15] exhibit mixed-valent ground states with halogen- and metal-sublattice dimerization, respectively.[16,17] Photo- and pressure-induced phase transitions[18,19,20] are feasible in the former, while successive phase transitions[15,17,21] occur with decreasing temperature in the latter.

Several chemists[22] have recently made a brandnew attempt to fabricate MX ladder materials and obtained $(bpym)[Pt(en)X]_2(ClO_4)_4{\cdot}2H_2O$ ($X = Cl, Br, I$; en = ethylenediamine = $C_2H_8N_2$; bpym = bipyrimidine = $C_8H_6N_4$), which comprise double-chain platinum complexes with intrachain bridging halogen ions and interchain bridging bipyrimidine molecules. A wider variety of mixed-valent states and their competition with Mott insulators are expected of such a geometric crystalline structure. $SrCu_2O_3$[23] and NaV_2O_5[24] have also been studied from a similar point of view. The former behaves as a strongly correlated multiband d-p ladder especially under hole doping,[25] while the latter is describable within a single-band Hamiltonian[26] but its d_{xy} electrons are possibly coupled to phonons originating in the apical and/or in-plane oxygen ions.[27,28] The newly synthesized MX ladder compounds are all the more fascinating in that d-p orbital hybridization and electron-lattice interaction are both relevant.

Thus motivated, we make our first attempt to reveal their ground-state properties making group-theoretical analyses and Hartree-Fock calculations. A symmetry argument[29,30,31] allows us to systematically derive density-wave solutions and reduce the following numerical efforts to the minimum necessary.[32] A mean-field approximation applied to low-dimensional systems tends to overstabilize broken-symmetry states against temperature[21,33] but plays a leading role in revealing possible ground states and interpreting their competition.[26,34,35,36,37,38] Hartree-Fock calculations of MMX chains[32] have indeed characterized the pop- and RCS_2-ligand complexes as d_{z^2}-single-band and d_{z^2}-p_z-hybridized two-band materials, respectively, elucidating their distinct ground states of mixed valence. Even the relaxation mechanism of photogenerated charge-transfer excitations in mixed-valent MX[39,40] and MMX[41] chains have been calculated consistently with experimental observations within the Hartree-Fock scheme. The synthesized PtX ladders look double-chain analogs of the conventional MX chain compounds $[Pt(en)_2X](ClO_4)_2$ and there are some similarities between their intrachain absorption spectra.[42] The Hartree-Fock scheme combined with a symmetry argument promises to give us a bird's-eye view of metal-halide ladders as well.

II. MODEL HAMILTONIAN AND ITS SYMMETRY PROPERTIES

We consider a fully dressed three-quarter-filled two-band Peierls-Hubbard Hamiltonian on the ladder lattice:

$$\mathcal{H} = \sum_{n,l,s}\Big\{\big[\varepsilon_M - \beta_M(u_{n:lX} - u_{n-1:lX})\big]n_{n:lMs} + \big[\varepsilon_X - \beta_X(u_{n+1:lM} - u_{n:lM})\big]n_{n:lXs}\Big\}$$
$$- \sum_{n,s}\Big\{\sum_l\big[t_{MX} + \alpha(u_{n:lM} - u_{n:lX})\big]a^\dagger_{n:lMs}a_{n:lXs} - \sum_l\big[t_{MX} - \alpha(u_{n:lM} - u_{n-1:lX})\big]a^\dagger_{n:lMs}a_{n-1:lXs}$$
$$+ t_{MM}a^\dagger_{n:1Ms}a_{n:2Ms} + \text{H.c.}\Big\} + \frac{K_{MX}}{2}\sum_{n,l}\big[(u_{n:lM} - u_{n:lX})^2 + (u_{n:lM} - u_{n-1:lX})^2\big]$$
$$+ \sum_{n,l}\sum_{A=M,X} U_A n_{n:lA\uparrow}n_{n:lA\downarrow} + \sum_{n,l,s,s'}\Big\{V^{\rm leg}_{MX}n_{n:lMs}(n_{n:lXs'} + n_{n-1:lXs'}) + V^{\rm diag}_{MX}n_{n:lMs}(n_{n:\bar{l}Xs'} + n_{n-1:\bar{l}Xs'})\Big\}$$
$$+ \sum_{n,s,s'}\sum_{A=M,X}\Big\{V^{\rm rung}_{AA}n_{n:1As}n_{n:2As'} + V^{\rm diag}_{AA}n_{n:1As}(n_{n-1:2As'} + n_{n+1:2As'}) + \sum_l V^{\rm leg}_{AA}n_{n:lAs}n_{n-1:lAs'}\Big\}, \qquad (2.1)$$

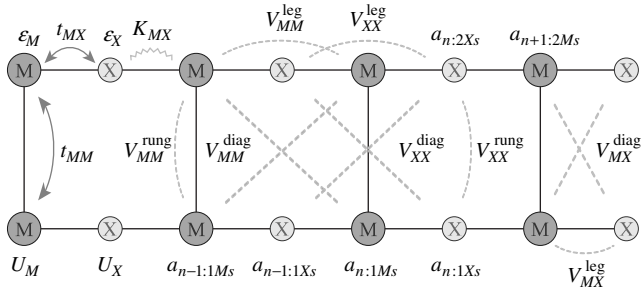

FIG. 1: The two-band extended Peierls-Hubbard modeling of the MX ladder.

where $n_{n:lAs} = a^\dagger_{n:lAs}a_{n:lAs}$ ($n = 1, 2, \cdots, N$; $l = 1, 2$; $A = M, X$; $s =\uparrow, \downarrow$) with $a^\dagger_{n:lAs}$ creating an electron with spin s for the Md_{z^2} ($A = M$) or Xp_z ($A = X$) orbital on the lth leg in the nth unit, while $u_{n:lA}$ is the leg-direction displacement of the metal ($A = M$) or halogen ($A = X$) on the lth leg in the nth unit from its equilibrium position. α and β_A describe the Peierls- and Holstein-type electron-lattice couplings, respectively, with K_{MX} being the metal-halogen spring constant. Coulomb interactions are taken into consideration up to next-nearest-neighbor metals and halogens, which is necessary and sufficient considering that the intrachain and interchain metal spacings are almost equal.[22] Those between every pair of metals diagonally facing to each other, $V^{\rm diag}_{MM}$, play a key role in controlling the interchain charge arrangement. A similar modeling has been applied to CuO d-p ladders.[43] The notation is further explained in Fig. 1.

When we consider normal states, the symmetry group of any lattice electron system may be written as $\mathbf{G} = \mathbf{P} \times \mathbf{S} \times \mathbf{T}$, where $\mathbf{P}$, $\mathbf{S}$ and $\mathbf{T}$ are the groups of space, spin rotation and time reversal, respectively. For the present d_{z^2}-p_z ladder $\mathbf{P}$ reads $\mathbf{L} \wedge \mathbf{D}_2$, where $\mathbf{D}_2 = \{E, C_{2z}, C_{2y}, C_{2x}\}$ and $\mathbf{L} = \{E, l\}$ with l being the one-dimensional translation by a unit cell. Defining the Fourier transformation as $a^\dagger_{k:lMs} = N^{-1/2}\sum_n \mathrm{e}^{\mathrm{i}kn}a^\dagger_{n:lMs}$ and $a^\dagger_{k:lXs} = N^{-1/2}\sum_n \mathrm{e}^{\mathrm{i}k(n+1/2)}a^\dagger_{n:lXs}$ with the lattice constant along the legs set equal to unity, we analyze all the irreducible real representations of $\mathbf{G}$, which are referred to as $\check{G}$, on the Hermitian-operator bases $\{a^\dagger_{k:lAs}a_{k':l'A's'}\}$. Actions of the space group elements on the electron operators are given in Table I, whereas those of $u(\boldsymbol{e}, \theta) = \sigma^0\cos(\theta/2) - (\boldsymbol{\sigma}\cdot\boldsymbol{e})\sin(\theta/2) \in \mathbf{S}$ and $t \in \mathbf{T}$ are defined as $u(\boldsymbol{e}, \theta)\cdot a^\dagger_{k:lAs} = \sum_{s'}[u(\boldsymbol{e}, \theta)]_{ss'}a^\dagger_{k:lAs'}$ and $t \cdot a^\dagger_{k:lAs} = (-1)^{\delta_{s\uparrow}}a^\dagger_{-k:lA-s}$, respectively, where σ^0 and $\boldsymbol{\sigma} = (\sigma^x, \sigma^y, \sigma^z)$ are the 2×2 unit matrix and a vector composed of the Pauli matrices, respectively. There is a one-to-one correspondence between $\check{G}$ and broken-symmetry phases of density-wave type.[44] Any representation $\check{G}$ is obtained as a Kronecker product of the irreducible real representations of $\mathbf{P}$, $\mathbf{S}$ and $\mathbf{T}$: $\check{G} = \check{P}\otimes\check{S}\otimes\check{T}$. $\check{P}$ is characterized by an ordering vector q in the Brillouin zone and an irreducible representation of its little group $\mathbf{P}(q)$, and is therefore labeled $q\check{P}(q)$. The relevant representations of $\mathbf{S}$ are given by $\check{S}^0(u(\boldsymbol{e}, \theta)) = 1$ (nonmagnetic) and $\check{S}^1(u(\boldsymbol{e}, \theta)) = O(u(\boldsymbol{e}, \theta))$ (magnetic), where $O(u(\boldsymbol{e}, \theta))$ is the 3×3 orthogonal matrix satisfying $u(\boldsymbol{e}, \theta)\boldsymbol{\sigma}^\lambda u^\dagger(\boldsymbol{e}, \theta) = \sum_{\mu=x,y,z}[O(u(\boldsymbol{e}, \theta))]_{\lambda\mu}\boldsymbol{\sigma}^\mu$ ($\lambda = x, y, z$), whereas those of $\mathbf{T}$ by $\check{T}^0(t) = 1$ (symmetric) and $\check{T}^1(t) = -1$ (antisymmetric). The representations $\check{P}\otimes\check{S}^0\otimes\check{T}^0$, $\check{P}\otimes\check{S}^1\otimes\check{T}^1$, $\check{P}\otimes\check{S}^0\otimes\check{T}^1$ and $\check{P}\otimes\check{S}^1\otimes\check{T}^0$ correspond to charge-density-wave (CDW), spin-density-wave (SDW), charge-current-wave (CCW) and spin-current-wave (SCW) states, respectively.

We investigate static density waves of $q = 0$ and $q = \pi$, which are labeled Γ and X, respectively. Then the Hamiltonian (2.1) is rewritten within the Hartree-Fock scheme as

$$\mathcal{H}_{\rm HF} = \sum_{lA,l'A'}\sum_{K=\Gamma,X}\sum_{\lambda=0,x,y,z}\sum_{k,s,s'} x^\lambda_{lAl'A'}(K;k) \times a^\dagger_{k+q(K):lAs}a_{k:l'A's'}\sigma^\lambda_{ss'}, \qquad (2.2)$$

where $q(\Gamma) = 0$ and $q(X) = \pi$. $x^\lambda_{lAl'A'}(K;k)$ can be expressed in terms of density matrices $\rho^\lambda_{l'A'lA}(K;k) = \sum_{s,s'}\langle a^\dagger_{k+q(K):lAs}a_{k:l'A's'}\rangle_{\rm HF}\sigma^\lambda_{ss'}/2$, where $\langle\cdots\rangle_{\rm HF}$ denotes the quantum average in a Hartree-Fock eigenstate, and is determined self-consistently. Since $\mathbf{P}(\Gamma) =$

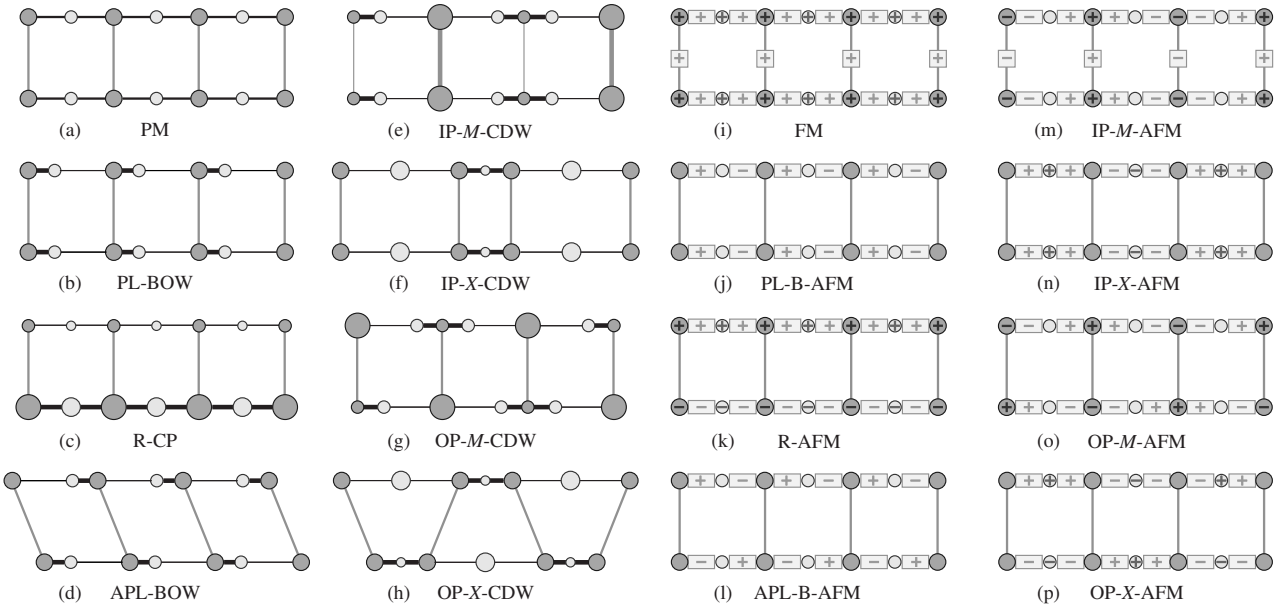

FIG. 2: Schematic representation of possible density-wave states, where the various circles and segments describe the variation of local charge densities $\sum_s \langle a^\dagger_{n:lAs} a_{n:lAs}\rangle_{\rm HF}$ and bond orders $\sum_s \langle a^\dagger_{n:lAs} a_{n':l'A's}\rangle_{\rm HF}$, respectively, whereas the signs $\pm$ in circles and strips denote the alternation of local spin densities $\sum_s \langle a^\dagger_{n:lAs} a_{n:lAs}\rangle_{\rm HF}\sigma^z_{ss}/2$ and spin bond orders $\sum_s \langle a^\dagger_{n:lAs} a_{n':l'A's}\rangle_{\rm HF}\sigma^z_{ss}/2$, respectively. Circles shifted from the regular position signify lattice distortion, which is peculiar to nonmagnetic phases.

$\mathbf{P}(X) = \mathbf{D}_2$, $\check{P}(\Gamma)$ and $\check{P}(X)$ are both given by the irreducible representations of $\mathbf{D}_2$, which are listed with their characters in Table II. Via group operations, the Hamiltonian (2.2) is further decomposed into symmetry-definite irreducible components as

$$\mathcal{H}_{\rm HF} = \sum_{K=\Gamma,X} \sum_{R=A_1,A_2,B_1,B_2} \sum_{\lambda=0,z} \sum_{\tau=0,1} h^{\lambda\tau}_{KR}, \qquad (2.3)$$

where $h^{\lambda\tau}_{KR}$ is given by

$$h^{\lambda\tau}_{KR} = \frac{d^R}{2g} \sum_{t\in\mathbf{T}} \check{T}^\tau(t) \sum_{p\in\mathbf{D}_2} \chi^R(p) \sum_{lA,l'A'} \sum_{k,s,s'} tp \cdot x^\lambda_{lAl'A'}(K;k) a^\dagger_{k+q(K):lAs} a_{k:l'A's'} \sigma^\lambda_{ss'}. \qquad (2.4)$$

$\chi^R(p)$ is the irreducible character of the R representation for the group element p, $g\,(=4)$ is the order of $\mathbf{D}_2$ and $d^R\,(=1)$ is the dimension of R. No representation of $d^R = 1$ gives a helical SDW solution ($\lambda = x, y$). The broken-symmetry Hamiltonians for $KR \otimes \check{S}^0 \otimes \check{T}^0$ and $KR \otimes \check{S}^1 \otimes \check{T}^1$ read $h^{00}_{\Gamma A_1} + h^{00}_{KR}$ and $h^{00}_{\Gamma A_1} + h^{z1}_{KR}$, respectively. The lattice distortion $u_{n:lA}$ is determined so as to minimize the Hartree-Fock energy $\langle\mathcal{H}\rangle_{\rm HF}$ and is also described in terms of density matrices. Considering that density matrices have the same symmetry properties as their host Hamiltonian, we can qualitatively characterize all the density-wave solutions, which are summarized in the following and illustrated in Fig. 2:

(a) $\Gamma A_1 \otimes \check{S}^0 \otimes \check{T}^0$: The paramagnetic state with the full symmetry $\mathbf{G}$, abbreviated as PM.

(b) $\Gamma A_2 \otimes \check{S}^0 \otimes \check{T}^0$: Parallel bond order waves with the halogen sublattice distorted, abbreviated as PL-BOW.

(c) $\Gamma B_1 \otimes \check{S}^0 \otimes \check{T}^0$: Polarized charge densities on rungs, abbreviated as R-CP.

(d) $\Gamma B_2 \otimes \check{S}^0 \otimes \check{T}^0$: Antiparallel bond order waves with the halogen sublattice distorted, abbreviated as APL-BOW.

(e) $XA_1 \otimes \check{S}^0 \otimes \check{T}^0$: Charge density waves in phase on the metal sublattice with the halogen sublattice dis-

TABLE I: The space group actions on the electron operators.

	l	C_{2z}	C_{2y}	C_{2x}
$a^\dagger_{k:1Ms}$	$e^{-ik}a^\dagger_{k:1Ms}$	$a^\dagger_{k:2Ms}$	$a^\dagger_{-k:1Ms}$	$a^\dagger_{-k:2Ms}$
$a^\dagger_{k:2Ms}$	$e^{-ik}a^\dagger_{k:2Ms}$	$a^\dagger_{k:1Ms}$	$a^\dagger_{-k:2Ms}$	$a^\dagger_{-k:1Ms}$
$a^\dagger_{k:1Xs}$	$e^{-ik}a^\dagger_{k:1Xs}$	$a^\dagger_{k:2Xs}$	$-a^\dagger_{-k:1Xs}$	$-a^\dagger_{-k:2Xs}$
$a^\dagger_{k:2Xs}$	$e^{-ik}a^\dagger_{k:2Xs}$	$a^\dagger_{k:1Xs}$	$-a^\dagger_{-k:2Xs}$	$-a^\dagger_{-k:1Xs}$
$a^\dagger_{k+\pi:1Ms}$	$-e^{-ik}a^\dagger_{k+\pi:1Ms}$	$a^\dagger_{k+\pi:2Ms}$	$a^\dagger_{-k+\pi:1Ms}$	$a^\dagger_{-k+\pi:2Ms}$
$a^\dagger_{k+\pi:2Ms}$	$-e^{-ik}a^\dagger_{k+\pi:2Ms}$	$a^\dagger_{k+\pi:1Ms}$	$a^\dagger_{-k+\pi:2Ms}$	$a^\dagger_{-k+\pi:1Ms}$
$a^\dagger_{k+\pi:1Xs}$	$-e^{-ik}a^\dagger_{k+\pi:1Xs}$	$a^\dagger_{k+\pi:2Xs}$	$a^\dagger_{-k+\pi:1Xs}$	$a^\dagger_{-k+\pi:2Xs}$
$a^\dagger_{k+\pi:2Xs}$	$-e^{-ik}a^\dagger_{k+\pi:2Xs}$	$a^\dagger_{k+\pi:1Xs}$	$a^\dagger_{-k+\pi:2Xs}$	$a^\dagger_{-k+\pi:1Xs}$

TABLE II: Irreducible representations and characters for $\mathbf{D}_2$.

$\mathbf{D}_2$	Basis	E	C_{2z}	C_{2y}	C_{2x}
A_1	x^2, y^2, z^2	1	1	1	1
A_2	xy	1	1	−1	−1
B_1	xz	1	−1	1	−1
B_2	yz	1	−1	−1	1

torted, abbreviated as IP-M-CDW.

(f) $XA_2 \otimes \check{S}^0 \otimes \check{T}^0$: Charge density waves in phase on the halogen sublattice with the metal sublattice distorted, abbreviated as IP-X-CDW.

(g) $XB_1 \otimes \check{S}^0 \otimes \check{T}^0$: Charge density waves out of phase on the metal sublattice with the halogen sublattice distorted, abbreviated as OP-M-CDW.

(h) $XB_2 \otimes \check{S}^0 \otimes \check{T}^0$: Charge density waves out of phase on the halogen sublattice with the metal sublattice distorted, abbreviated as OP-X-CDW.

(i) $\Gamma A_1 \otimes \check{S}^1 \otimes \check{T}^1$: Ferromagnetism on both metal and halogen sublattices, abbreviated as FM.

(j) $\Gamma A_2 \otimes \check{S}^1 \otimes \check{T}^1$: Bond-centered antiferromagnetic spin densities on legs parallel to each other, abbreviated as PL-B-AFM.

(k) $\Gamma B_1 \otimes \check{S}^1 \otimes \check{T}^1$: Antiferromagnetic spin densities on rungs, abbreviated as R-AFM.

(l) $\Gamma B_2 \otimes \check{S}^1 \otimes \check{T}^1$: Antiparallel spin bond order waves, abbreviated as APL-B-AFM.

(m) $XA_1 \otimes \check{S}^1 \otimes \check{T}^1$: Antiferromagnetic spin densities in phase on the metal sublattice, abbreviated as IP-M-AFM.

(n) $XA_2 \otimes \check{S}^1 \otimes \check{T}^1$: Antiferromagnetic spin densities in phase on the halogen sublattice, abbreviated as IP-X-AFM.

(o) $XB_1 \otimes \check{S}^1 \otimes \check{T}^1$: Antiferromagnetic spin densities out of phase on the metal sublattice, abbreviated as OP-M-AFM.

(p) $XB_2 \otimes \check{S}^1 \otimes \check{T}^1$: Antiferromagnetic spin densities out of phase on the halogen sublattice, abbreviated as OP-X-AFM.

III. GROUND-STATE PHASE DIAGRAMS

The translationally dimerized phases (e)-(h) and (m)-(p) may be expected to appear at zero temperature. PtX chain compounds exhibit a ground state of the M-CDW type, while NiX ones exhibit that of the M-AFM type. When the chains are coupled in pairs, we wonder how their density waves are stabilized in the ground state, in phase (IP) or out of phase (OP) with each other. We take another interest in whether or not a density wave may appear in the X, rather than M, sublattice. In order to visualize ground-state phase competition, we numerically calculate $\langle \mathcal{H} \rangle_{\rm HF}$ for all the broken-symmetry phases at a sufficiently low temperature ($k_{\rm B}T/t_{\rm MX} = 0.05$) in the thermodynamic limit ($N \to \infty$).

Considering that the on-site Coulomb repulsion may vary with the constituent metals and halogens as $U_{\rm Pt} < U_{\rm Pd} < U_{\rm Ni}$ and $U_{\rm I} < U_{\rm Br} < U_{\rm Cl}$, we draw several ground-state phase diagrams on the U_M-U_X plane in Fig. 3, where the electronic and phononic energies are scaled by t_{MX} and K_{MX}, respectively. A variety of Peierls and Mott insulators are stabilized at moderate and strong Coulomb interactions, respectively. Charge or spin densities oscillate in the M sublattice for $U_X \lesssim U_M$, whereas in the X sublattice for $U_M \lesssim U_X$. AFM phases of the

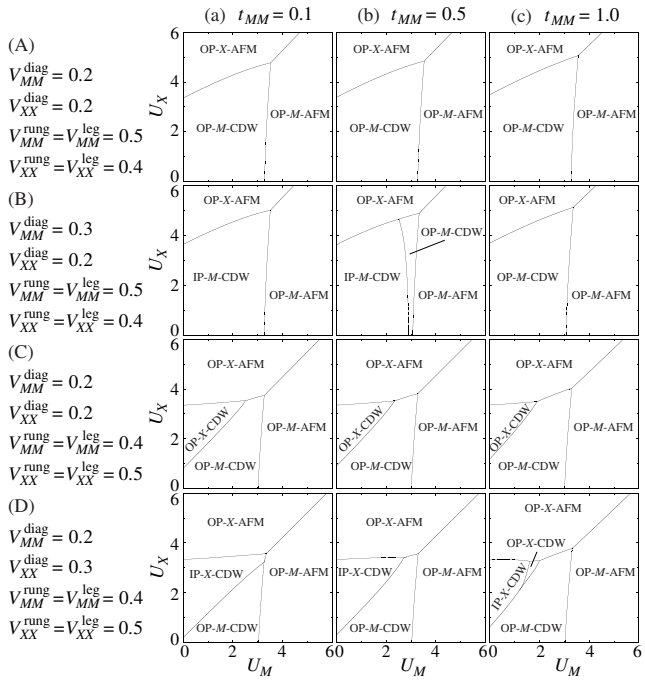

FIG. 3: Ground-state phase diagrams, where $\varepsilon_M - \varepsilon_X = 1.0$, $\alpha = 0.1$, $\beta_M = \beta_X = 1.0$, $V_{MX}^{\rm leg} = 1.0$ and $V_{MX}^{\rm diag} = 0.4$ in common.

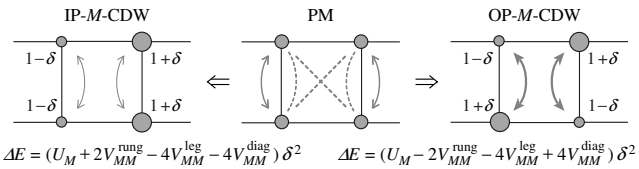

FIG. 4: A simple consideration of the competition between IP-M-CDW and OP-M-CDW. The Coulomb energy gains due to charge disproportionation, ΔE, are evaluated, provided the X p_z orbitals are fully filled and thus negligible.

IP type are hardly stabilized, while CDW phases of the IP and OP types closely compete with each other with varying $V_{AA}^{\rm rung}$, $V_{AA}^{\rm diag}$ and t_{MM}. The present AFM phase boundaries should be refined beyond the Hartree-Fock scheme when NiX ladders are synthesized, where quantum correlations are supposed to be significant.[45] Any AFM phase might be stabilized with weak but nonnegligible interactions between neighboring ladders.

Figures 3(A) and 3(B) demonstrate the competition between the most likely phases IP-M-CDW and OP-M-CDW on condition that the inter-metal Coulomb interactions are slightly larger than the inter-halogen ones, which is understandable within the naivest consideration of d-electron correlations. Figure 4 shows that the two states may be balanced at $V_{MM}^{\rm rung} \simeq 2V_{MM}^{\rm diag}$. Indeed, there appears OP-M-CDW at $2V_{MM}^{\rm diag} = 0.4 < 0.5 = V_{MM}^{\rm rung}$, while IP-$M$-CDW at $2V_{MM}^{\rm diag} = 0.6 > 0.5 = V_{MM}^{\rm rung}$. It is also interesting to observe the phase competition from the viewpoint of electron itinerancy. While IP-M-CDW and OP-M-CDW are degenerate to each other in decou-

pled chains, the interchain electron hopping is much more advantageous to OP-M-CDW. Once t_{MM} is on, IP-M-CDW and OP-M-CDW are both stabilized by an energy $\propto t_{MM}^2$ in general, but the latter gains much more. If we think of the limit of $\delta = 1$, IP-M-CDW gains no energy with increasing t_{MM}. That is why IP-M-CDW is replaced by OP-M-CDW in Fig. 3(B-c).

Figures 3(C) and 3(D) reveal a possibility of the novel phases IP-X-CDW and OP-X-CDW appearing on condition that the inter-metal Coulomb interactions are slightly smaller than the inter-halogen ones. IP-X-CDW and OP-X-CDW also compete with each other, the former of which is stabilized by $V_{XX}^{\rm diag}$, while the latter of which by $V_{XX}^{\rm rung}$. The hybridization-driven phase competition was predicted for single chains[32,46,47,48] as well and was indeed observed in an MMX compound.[17] Since U_X acts on the oxidation of X^- ions, it is interesting to tune PtCl ladders chemically, with varying ligands, for example, and physically, by applying pressure, for instance.

IV. SUMMARY

Charge- or spin-ordered states of the MX ladder are thus various and highly competing. Raman spectra for (bpym)[Pt(en)X]$_2$(ClO$_4$)$_4$·2H$_2$O suggest a mixed-valent ground state of Pt$^{\rm II}$ and Pt$^{\rm IV}$,[42] we are for the moment encouraged to identify it as either IP-M-CDW or OP-M-CDW. In any case, it is highly interesting to apply pressure to the materials. Sample size reduction along the rungs enhances t_{MM}, whereas that along the legs effectively reduces t_{MM}. Our findings claim that there is a good possibility of pressure-induced phase transitions between IP-M-CDW and OP-M-CDW.

Further phase transitions may be expected at finite temperatures and/or under doping. Photoexcitations and their nonlinear relaxation processes must be the following interest. We hope the present study will stimulate and guide further explorations into the brandnew MX materials.

Acknowledgments

The authors thank K. Iwano, H. Okamoto and M. Yamashita for fruitful discussions. This work was supported by the Ministry of Education, Culture, Sports, Science and Technology of Japan.

[1] J. T. Gammel, A. Saxena, I. Batistić, A. R. Bishop and S. R. Phillpot: Phys. Rev. B **45** (1992) 6408.
[2] S. W. Weber-Milbrodt, J. T. Gammel, A. R. Bishop and E. Y. Loh, Jr.: Phys. Rev. B **45** (1992) 6435.
[3] H. Reihlen and E. Flohr: Ber. Dtsch. Chem. Ges. **67** (1934) 2010.
[4] R. J. H. Clark, M. L. Franks and W. R. Trumble: Chem. Phys. Lett. **41** (1976) 287.
[5] H. Tanino and K. Kobayashi: J. Phys. Soc. Jpn. **52** (1983) 1446.
[6] H. Toftlund and O. Simonsen: Inorg. Chem. **23** (1984) 4261.
[7] K. Toriumi, Y. Wada, T. Mitani, S. Bandow, M. Yamashita and Y. Fujii: J. Am. Chem. Soc. **111** (1989) 2341.
[8] H. Okamoto, K. Okaniwa, T. Mitani, K. Toriumi and M. Yamashita: Solid State Commun. **77** (1991) 465.
[9] K. Nasu: J. Phys. Soc. Jpn. **52** (1983) 3865; **53** (1984) 302; **53** (1984) 427.
[10] K. Marumoto, H. Tanaka, S. Kuroda, T. Manabe and M. Yamashita: Phys. Rev. B **60** (1999) 7699.
[11] Y. Wakabayashi, N. Wakabayashi, M. Yamashita, T. Manabe and N. Matsushita: J. Phys. Soc. Jpn. **68** (1999) 3948.
[12] C.-M. Che, F. H. Herbstein, W. P. Schaefer, R. E. Marsh and H. B. Gray: J. Am. Chem. Soc. **105** (1983) 4604.
[13] R. J. H. Clark, M. Kurmoo, H. M. Dawes and M. B. Hursthouse: Inorg. Chem. **25** (1986) 409.
[14] C. Bellitto, A. Flamini, L. Gastaldi and L. Scaramuzza: Inorg. Chem. **22** (1983) 444.
[15] S. Ikeuchi, K. Saito, Y. Nakazawa, M. Mitsumi, K. Toriumi and M. Sorai: J. Phys. Chem. B **108** (2004) 387.
[16] L. G. Butler, M. H. Zietlow, C.-M. Che, W. P. Schaefer, S. Sridhar, P. J. Grunthaner, B. I. Swanson, R. J. H. Clark and H. B. Gray: J. Am. Chem. Soc. **110** (1988) 1155.
[17] H. Kitagawa, N. Onodera, T. Sonoyama, M. Yamamoto, T. Fukawa, T. Mitani, M. Seto and Y. Maeda: J. Am. Chem. Soc. **121** (1999) 10068.
[18] H. Matsuzaki, T. Matsuoka, H. Kishida, K. Takizawa, H. Miyasaka, K. Sugiura, M. Yamashita and H. Okamoto: Phys. Rev. Lett. **90** (2003) 046401.
[19] S. Yamamoto: Phys. Rev. B **64** (2001) 140102(R).
[20] K. Yonemitsu and N. Miyashita: Phys. Rev. B **68** (2003) 075113.
[21] S. Yamamoto: J. Phys. Soc. Jpn. **70** (2001) 1198.
[22] M. Yamashita, D. Kawakami, S. Matsunaga, S. Takaishi, H. Miyasaka and K. Sugiura: private communication.
[23] Z. Hiroi and M. Takano: Nature **377** (1995) 41.
[24] M. Isobe and Y. Ueda: J. Phys. Soc. Jpn. **65** (1996) 1178.
[25] N. Ueda and T. Mizokawa: Phys. Rev. B **69** (2004) 224406.
[26] H. Seo and H. Fukuyama: J. Phys. Soc. Jpn. **67** (1998) 2602.
[27] J. Riera and D. Poilblanc: Phys. Rev. B **59** (1999) 2667.
[28] E. Y. Sherman, M. Fischer, P. Lemmens, P. H. M. van Loosdrecht and G. Güntherodt: Europhys. Lett. **48** (1999) 648.
[29] S. Yamamoto and M. Ozaki: Solid State Commun. **83** (1992) 329; **83** (1992) 335.
[30] S. Yamamoto: Phys. Lett. A **258** (1999) 183.
[31] A. Masago and N. Suzuki: J. Phys. Soc. Jpn. **73** (2004) 2523.
[32] S. Yamamoto, Phys. Rev. B **63**, 125124 (2001).
[33] K. Kishigi: J. Phys. Soc. Jpn. **67** (1998) 3825.
[34] H. Kino and H. Fukuyama: J. Phys. Soc. Jpn. **64** (1995) 1877; **64** (1995) 2726; **64** (1995) 4523; **65** (1996) 2158.
[35] H. Seo and H. Fukuyama: J. Phys. Soc. Jpn. **66** (1997)

3352; **67** (1998) 1848.
[36] H. Seo and H. Fukuyama: J. Phys. Soc. Jpn. **66** (1997) 1249.
[37] N. Kobayashi, M. Ogata and K. Yonemitsu: J. Phys. Soc. Jpn. **67** (1998) 1098.
[38] S. Yamamoto: J. Phys. Soc. Jpn. **69** (2000) 13.
[39] A. Mishima and K. Nasu: Phys. Rev. B **39** (1989) 5758; **39** (1989) 5763.
[40] K. Iwano: J. Phys. Soc. Jpn. **66** (1997) 1088.
[41] J. Ohara and S. Yamamoto: Phys. Rev. B **73** (2006) 045122.
[42] H. Matsuzaki, H. Kishida and H. Okamoto: private communication.
[43] S. Nishimoto, E. Jeckelmann and D. J. Scalapino: Phys. Rev. B **66** (2002) 245109.
[44] M. Ozaki: J. Math. Phys. **26** (1998) 1514; **26** (1998) 1521.
[45] J. Ohara and S. Yamamoto: J. Phys. Chem. Solids **66** (2005) 1571.
[46] H. Röder, A. R. Bishop and T. Gammel: Phys. Rev. Lett. **70** (1993) 3498.
[47] S. Yamamoto: Phys. Lett. A **247** (1998) 422.
[48] M. Kuwabara and K. Yonemitsu: J. Mater. Chem. **11** (2001) 2163.